

Zone-boundary excitations in coupled Haldane spin chain compounds $\text{PbNi}_2\text{V}_2\text{O}_8$ and $\text{SrNi}_2\text{V}_2\text{O}_8$

A. Zheludev*

Physics Department, Brookhaven National Laboratory, Upton, New York 11973

T. Masuda and K. Uchinokura

Department of Advanced Materials Science and Department of Applied Physics, The University of Tokyo, Tokyo 113-8656, Japan

S. E. Nagler

Oak Ridge National Laboratory, Bld. 7692, MS 6393, P.O. Box 2008, Oak Ridge, Tennessee 37831

(Received 26 March 2001; published 12 September 2001)

Magnetic excitations in the quasi-one-dimensional quantum antiferromagnets $\text{PbNi}_2\text{V}_2\text{O}_8$ and $\text{SrNi}_2\text{V}_2\text{O}_8$ are measured all the way up to the zone-boundary energy using inelastic neutron scattering from powder samples. An estimate for next-nearest-neighbor in-chain interactions is obtained. The role played by these interactions in spin-vacancy-induced magnetic ordering in $\text{PbNi}_2\text{V}_2\text{O}_8$ is discussed.

DOI: 10.1103/PhysRevB.64.134415

PACS number(s): 75.30.Ds, 75.50.Ee, 75.40.Gb

I. INTRODUCTION

The quasi-one-dimensional (quasi-1D) $S=1$ antiferromagnet (AF) $\text{PbNi}_2\text{V}_2\text{O}_8$ was recently shown to be the first example of a Haldane-gap system¹ to undergo long-range magnetic ordering upon doping with nonmagnetic impurities.^{2,3} This unique behavior was understood through inelastic neutron scattering measurements, which suggested that three-dimensional (3D) interchain interactions in $\text{PbNi}_2\text{V}_2\text{O}_8$ are almost (but not quite) strong enough to destroy the Haldane singlet ground state even in the undoped material.^{2,4} In fact, in the very similar isostructural compound $\text{SrNi}_2\text{V}_2\text{O}_8$, interchain coupling exceeds the critical value, and, unlike the Pb-based material, the undoped Sr-Ni vanadate orders magnetically at $T=7$ K.^{2,4}

The introduction of nonmagnetic vacancies into gapped quantum spin chains produces free $S=1/2$ degrees of freedom on either side of each impurity site.⁵⁻⁸ In the presence of arbitrarily weak interchain interactions, these free spins will order in three dimensions at sufficiently low temperature. However, next-nearest-neighbor (NNN) interactions within the chains can prevent this from happening.⁹ Naively, in the presence of AF NNN coupling, one can expect the liberated spins around each impurity to bind into nonmagnetic singlets (dimers), preserving the disordered ground state of the system.

There are at least two indications that NNN interactions may be active in $\text{PbNi}_2\text{V}_2\text{O}_8$ and $\text{SrNi}_2\text{V}_2\text{O}_8$. First, the spin chains in both materials are not linear, but are formed by Ni^{2+} ions arranged in four-step *spirals* propagating along the c axis of the orthorhombic lattice (for a detailed discussion of chain geometry and interchain interactions see Ref. 4). In this “twisted” structure NNN superexchange pathways involving equatorial oxygens of the NiO_6 tetrahedra can be quite effective. Second, there remains some discrepancy between the in-chain exchange constant J deduced from the Haldane gaps measured with neutron scattering, assuming only nearest-neighbor (NN) interactions ($J=9.0$ meV), and

from high-temperature ($T \approx J$) susceptibility data ($J=8.2$ meV). The former technique probes low-energy excitations around $q_{\parallel} = \pi$ (AF zone center), while the latter is sensitive to excitations in the entire Brillouin zone. The mismatch may be interpreted in terms of an additional coupling with a characteristic interaction length of twice the spin-spin separation in the chains, which is known to have different effects on zone-center and zone-boundary excitation energies.

The most direct way to resolve this issue would be to measure the dispersion of magnetic excitations in the entire Brillouin zone in a single-crystal sample. Unfortunately, no single-crystal or aligned powder samples of either $\text{PbNi}_2\text{V}_2\text{O}_8$ or $\text{SrNi}_2\text{V}_2\text{O}_8$, suitable for inelastic neutron scattering studies, are available to date. As will be discussed below, some information on NNN coupling can be obtained using powder samples if the measurements are extended all the way to the zone-boundary energy. Previous neutron scattering studies employed cold neutrons to investigate low-energy excitations in the two compounds.^{2,4} In the present paper we report thermal-neutron studies specifically aimed at measuring high-energy excitations. We then engage in a semiquantitative discussion of the role NNN interactions play in vacancy-induced ordering of weakly coupled Haldane spin chains and apply the results to the particular case of $\text{PbNi}_2\text{V}_2\text{O}_8$.

II. EXPERIMENTAL PROCEDURES AND RESULTS

Both vanadates crystallize in tetragonal structure, space group $I41cd$, with lattice constants $a=12.249(3)$ Å and $c=8.354(2)$ Å for $\text{PbNi}_2\text{V}_2\text{O}_8$ (Ref. 10) and $a=12.1617$ Å and $c=8.1617$ Å for $\text{SrNi}_2\text{V}_2\text{O}_8$ (Ref. 11), respectively. All measurements were performed on large (≈ 5 g) powder samples of $\text{PbNi}_2\text{V}_2\text{O}_8$ and $\text{SrNi}_2\text{V}_2\text{O}_8$, similar to those used in previous cold-neutron studies.⁴ The experiments were carried out at the HB3 three-axis spectrometer installed at the High Flux Isotope Reactor at Oak Ridge National Laboratory. Neutrons with a fixed final energy of 13.5 meV were used with a 5-cm-thick pyrolytic graphite (PG) filter

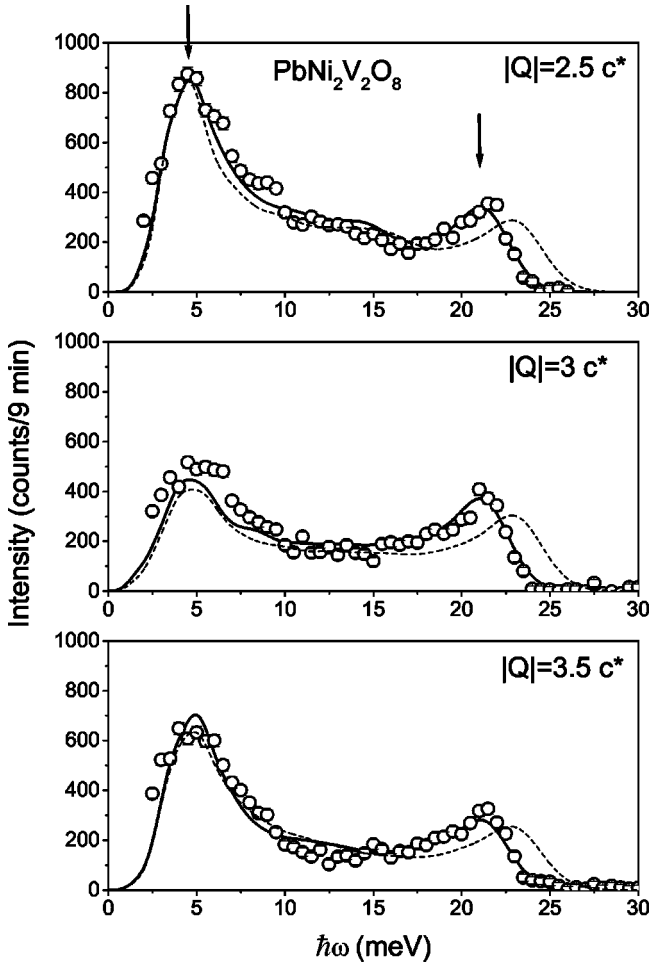


FIG. 1. Typical background-corrected constant- Q scans measured in $\text{PbNi}_2\text{V}_2\text{O}_8$ at $T=1.5$ K. Arrows roughly indicate the gap and zone-boundary energies. Solid lines are simulations based on the result of a semiglobal fit to the data, which allows for next-nearest-neighbor in-chain interactions, as described in the text. Dashed lines are a best fit assuming that only nearest-neighbor interactions are present. Statistical error bars are smaller than the symbol size.

positioned after the sample to eliminate higher-order beam contamination. PG(002) reflections were used for monochromator and analyzer, in combination with $48'-40'-40'-120'$ collimators. Sample environment was in all cases a standard ^4He -flow cryostat. The data were taken at $T=1.5$ K.

Typical data sets collected in constant- Q scans for $\text{PbNi}_2\text{V}_2\text{O}_8$ and $\text{SrNi}_2\text{V}_2\text{O}_8$ are shown in Fig. 1 and Fig. 2, respectively. Figure 3 shows the bulk of the data collected for the Sr system (only five scans, at $|Q|/c^*=2.5, 3, 3.5, 4,$ and $5,$ were collected for the Pb-based material). The measured intensities were scaled to correct for the previously determined energy-dependent $\lambda/2$ contribution to the incident beam, which affects the monitor rate. Within the incident neutron energy range used, the monitor efficiency changes by roughly 30%. In addition, a flat background (17 counts/min), measured at 30 meV energy transfer (above the magnetic excitation band), was subtracted from the data.

For both materials all scans have the characteristic

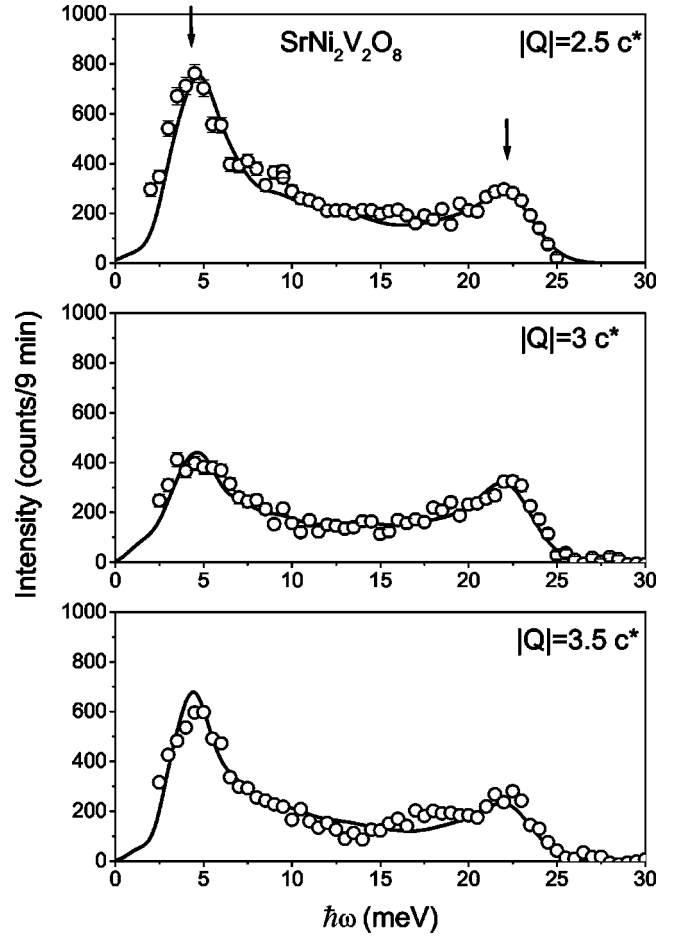


FIG. 2. Typical background-corrected constant- Q scans measured in $\text{SrNi}_2\text{V}_2\text{O}_8$ at $T=1.5$ K. Arrows and solid lines are as in Fig. 1. Statistical error bars are smaller than the symbol size.

M shape. In a powder sample one measures the spherical average of the dynamic structure factor $S(\mathbf{Q}, \omega)$. For large momentum transfers, a large portion of \mathbf{Q} space is sampled simultaneously, and the powder cross section is in many ways similar to the density-of-states function $n(\omega)$. In particular, one expects to see a peak in the powder cross section wherever the density of states is large, i.e., at the gap energy and at the zone boundary. As discussed previously,⁴ the peak around 5 meV energy transfer corresponds to excitations close to the Haldane gap at a momentum transfer $q_{\parallel} = \pi$

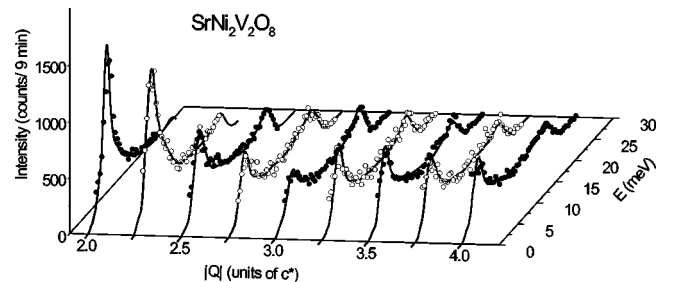


FIG. 3. The bulk of constant- Q scans measured in $\text{SrNi}_2\text{V}_2\text{O}_8$ at $T=1.5$ K. Solid lines are as in Fig. 1. Statistical error bars are smaller than the symbol size.

$+2\pi n$ (n integer) along the chain axis. The weaker higher-energy peaks represent excitation near the top of the band, i.e., in the vicinity of $q_{\parallel} = \pi/2 + \pi n$ (n integer).

III. DATA ANALYSIS

A. Model cross section

The convoluted nature of inelastic powder data makes it notoriously difficult to interpret (for an example see Ref. 12, particularly Sec. IV). The only way to extract information on the dynamic structure factor from such measurements is to assume a “reasonable” model and refine the parameter values to best fit the data. The main assumption of the model used for $\text{PbNi}_2\text{V}_2\text{O}_8$ and $\text{SrNi}_2\text{V}_2\text{O}_8$ to date is that these compounds are described as weakly interacting $S=1$ AF chains with magnetic anisotropy. This picture is based on susceptibility, high-field, and specific heat measurements and is supported by the observed unique shape of constant- E neutron scans.² In the present work we shall adopt this model as well.

The form of the neutron scattering cross section for this model was derived in Ref. 4 and is written in the single-mode approximation (SMA). Interchain interactions were accounted for within the random phase approximation (RPA). This cross section function performed rather well in describing *low-energy* neutron data. Previous studies of other Haldane-gap compounds, such as NENP (Ref. 13) and CsNiCl_3 (Ref. 14), have demonstrated that the SMA is, in fact, applicable in most of the Brillouin zone. The previously derived SMA cross section [Eqs. (5)–(13) of Ref. 4] could thus be safely used in interpreting our high-energy results. However, the expression for the dispersion relation [Eqs. (14) and (15) of Ref. 4] had to be slightly modified. These modifications are discussed in the following paragraphs.

1. Isolated chains with nearest-neighbor interactions

In Ref. 4 the dispersion of excitations in noninteracting Haldane spin chains was assumed to be sinusoidal and symmetric around the classical AF zone boundary $q_{\parallel} = \pi/2$. In fact, since translational symmetry is not broken in the Haldane ground state, the excitation energy extrapolates to a larger value at $q_{\parallel} \rightarrow 0$ than at $q_{\parallel} \rightarrow \pi$.¹⁵ This effect can be taken into account empirically by including an extra term in the dispersion relation.¹³ The dynamic susceptibility of a single Haldane spin chain is then written as

$$\chi^{\beta\beta}(q_{\parallel}, \omega) = \chi_{\pi}^{\beta\beta} \frac{1 - \cos q_{\parallel}}{2} \frac{\Delta_{\beta\beta}^2}{(\hbar\omega_{q_{\parallel}}^{\beta\beta})^2 - (\hbar\omega + i\epsilon)^2}, \quad (1)$$

$$(\hbar\omega_{q_{\parallel}}^{\beta\beta})^2 = \Delta_{\beta\beta}^2 + v^2 \sin^2 q_{\parallel} + \alpha^2 \cos^2 \frac{q_{\parallel}}{2}. \quad (2)$$

In these formulas, which replace Eq. (22) in Ref. 4, $\Delta_{\beta\beta}$ is the gap energy for the Haldane-gap mode of a particular polarization $\beta\beta$, $\chi_{\pi}^{\beta\beta}$ is the static staggered susceptibility, and v is the spin-wave velocity. The spin chains $\text{PbNi}_2\text{V}_2\text{O}_8$ and $\text{SrNi}_2\text{V}_2\text{O}_8$ contain four equivalent spins per crystallographic period along the c axis. Throughout this work the

actual wave vector transfer will be denoted as $\mathbf{Q} = \hbar\mathbf{a}^* + k\mathbf{b}^* + l\mathbf{c}^*$. The symbol $q_{\parallel} \equiv \mathbf{Q}\mathbf{c}/4$ in Eq. (2) will stand for the reduced wave vector transfer along the chains.

The energetics of a Haldane-gap AF is by now very well established through numerical work by several authors.^{16–18} For an $S=1$ Heisenberg chain with single-ion anisotropy of type $D(S^z)^2$ the approximate values of parameters are as follows:

$$\Delta_{xx} = \Delta_{yy} \approx \langle \Delta \rangle - \frac{2}{3} D, \quad (3)$$

$$\Delta_{zz} \approx \langle \Delta \rangle + \frac{4}{3} D, \quad (4)$$

$$\langle \Delta \rangle \approx 0.41J, \quad (5)$$

$$v \approx 2.49J, \quad (6)$$

$$\chi_{\pi}^{\beta\beta} \approx 1.26 \frac{v}{\Delta_{\beta\beta}^2}. \quad (7)$$

The parameter α in Eq. (2) characterizes the asymmetry of the dispersion relation. Existing experimental data for NENP (Ref. 13) and CsNiCl_3 (Ref. 14) give $\alpha = 1.45J \approx 0.58v$ and $\alpha = 1.1J \approx 0.44v$, respectively. The latter result inspires more confidence, as it was obtained with a much higher experimental resolution and gives a dispersion relation very similar to that obtained by direct diagonalization in finite-length chains.¹⁵ Throughout the rest of the paper we shall assume α fixed at $\alpha \equiv 0.44v$.

2. Next-nearest-neighbor interactions

Next-nearest-neighbor in-chain interactions, which we believe can be relevant for $\text{PbNi}_2\text{V}_2\text{O}_8$ and $\text{SrNi}_2\text{V}_2\text{O}_8$, can be accounted for within the RPA. It is straightforward to verify that isotropic NNN coupling of magnitude J' gives an additional term on the right-hand side (RHS) of Eq. (2) that can be written as

$$\chi_{\pi}^{\beta\beta} \Delta_{\beta\beta}^2 J' \frac{1 - \cos q_{\parallel}}{2} \cos 2q_{\parallel}. \quad (8)$$

The primary effect of NNN interactions is to modify the gap energies:

$$\Delta_{\beta\beta}^2 = \Delta_{\beta\beta,0}^2 (1 + \chi_{\pi}^{\beta\beta} J'), \quad (9)$$

where $\Delta_{\beta\beta,0}$ are the gaps in the absence of NNN coupling. The relative effect of NN interactions on the zone-boundary energy and spin-wave velocity is considerably smaller, and can be ignored. To a good approximation, in analyzing the experimental data one can use the dispersion relation (2), but treat the gap energies and v as independent parameters, rather than assuming that the relation (6) is valid only in the case $J' = 0$. The ratio $\xi = v/\langle \Delta \rangle$ can then be determined and used to obtain an estimate for J' . From Eqs. (3)–(7) and (9) for $J' \ll J$ one gets

$$\xi \approx \xi_0 \left(1 - 9.33 \frac{J'}{J} \right). \quad (10)$$

Here $\xi_0 = v / \langle \Delta_0 \rangle \approx 6.07$ is equal to the equal-time correlation length in the absence of NNN coupling.

3. Interchain interactions

For the coupling geometry found in $\text{PbNi}_2\text{V}_2\text{O}_8$ and $\text{SrNi}_2\text{V}_2\text{O}_8$, switching on interchain interactions within the RPA gives an additional term

$$-\chi_{\pi}^{\beta\beta} \Delta_{\beta\beta}^2 J_1 \cos(\pi l/2) [\cos(\pi h) + \cos(\pi k)] \frac{(1 - \cos \pi l/2)}{2} \quad (11)$$

on the RHS of Eq. (2). In this formula, which corresponds to the last terms in Eqs. (14) and (15) of Ref. 4, J_1 is the magnitude of nearest-neighbor interchain interactions. For our present purposes, the possible small anisotropy of J_1 will be ignored.

B. Parameters for $\text{PbNi}_2\text{V}_2\text{O}_8$ and $\text{SrNi}_2\text{V}_2\text{O}_8$

Our understanding of the physics of $\text{PbNi}_2\text{V}_2\text{O}_8$ and $\text{SrNi}_2\text{V}_2\text{O}_8$ is based on knowledge of the following characteristics: the intrinsic gap energies Δ_{zz} and $\Delta_{xx} = \Delta_{yy}$, the magnitude of interchain interactions J_1 , and the spin-wave velocity v . Can these four parameters be unambiguously determined from the available experimental data?

First, consider those quantities that characterize low-energy excitations near $q_{\parallel} = \pi$. For $\text{PbNi}_2\text{V}_2\text{O}_8$ the actual minima of the 3D dispersion, $E_{\min, \beta\beta}$, were *independently* measured in high-field magnetization studies of *aligned* powder samples.^{2,4} These energies are directly related to $\Delta_{\beta\beta}$ and J_1 . The third experimental value needed to unambiguously “untangle” these three quantities was probed in previous high-resolution cold-neutron measurements.⁴ Indeed, the well-defined lower-energy 5 meV peak in constant- q powder scans is located approximately at the top of the dispersion band perpendicular to the chains at $q_{\parallel} = \pi$, and its position is directly related to $\Delta_{\beta\beta}$ and J_1 . From the combined high-field and neutron measurements $\Delta_{\beta\beta}$ and J_1 can thus be reliably determined within the established model. For $\text{PbNi}_2\text{V}_2\text{O}_8$ these parameters are $\Delta_{zz} = 3.1(3)$ meV, $\Delta_{xx} = \Delta_{yy} = 4.0(3)$ meV, and $J_1 = -0.17(2)$ meV.⁴

For $\text{SrNi}_2\text{V}_2\text{O}_8$, which is *ordered* at low temperature, the model of weakly coupled Haldane spin chains is, strictly speaking, not applicable. Nevertheless, as the ordered moment is expected to be very small, the model is still a good approximation, except in the direct proximity of the magnetic Bragg peaks. From the analysis of the low-energy powder spectrum for $\text{SrNi}_2\text{V}_2\text{O}_8$ the following parameters were previously determined: $\Delta_{zz} = 2.8(4)$ meV, $\Delta_{xx} = \Delta_{yy} = 3.9(3)$ meV, and $J_1 = -0.17(3)$ meV.⁴

The exact value of the remaining “high-energy” parameter v has little impact on the low-energy powder spectrum and was not treated as an independent variable in Ref. 4. In contrast, v determines the high-temperature magnetic susceptibility of the system, which, provided $k_B T \gg \Delta$, is insen-

sitive to the details of the low-energy spectrum. This type of experiments yields $v \approx 20.4$ meV for $\text{PbNi}_2\text{V}_2\text{O}_8$. The present study provides the most direct measure of the zone-boundary energy, and hence the spin-wave velocity v , defined by the location of the higher-energy peak and cutoff in the constant- q powder scans. In analyzing these data we shall use the cross section defined in Eqs. (5)–(13) of Ref. 4 in combination with the dispersion relation given by Eqs. (2) and (11) above, using only v as an adjustable parameter of the model.

C. Fits to experimental data

In the data analysis, the powder average of the parameterized cross section was calculated numerically using a Monte Carlo routine. The result was further numerically convoluted with the Q - E resolution function of the three-axis spectrometer, calculated in the Cooper-Nathans approximation.¹⁹ Performing a true global fit to the data, using a single set of parameters to describe all measured scans, was not possible because of the scattering-angle dependence of neutron transmission in the sample. In the experiments the cylindrical samples were mounted with the symmetry axis horizontal. This admittedly less-than-ideal geometry was used for purely technical reasons. In this low-symmetry configuration neutron absorption effects, due to appreciable incoherent cross sections of Ni and V nuclei, are difficult to take into account accurately. Transmission in the sample was studied by measuring the intensity of incoherent elastic scattering and found to change by $\approx 30\%$, depending on scattering geometry. Within each measured constant- Q scan (scattering-angle range of about 30°) this correction is small and could be ignored. However, in analyzing the entire data sets, collected in a broad range of momentum and energy transfers (scattering-angle range of over 60°), a separate intensity prefactor had to be used for each constant- Q scan. Thus, for each compound, the data were analyzed in a semi-global fit: a single adjustable parameter v was used to *simultaneously* describe all measured scans, each with its own adjustable prefactor. The parameters were refined to best fit the data using a least-squares algorithm.

Excellent fits were obtained with $v = 20.6(7)$ meV for $\text{PbNi}_2\text{V}_2\text{O}_8$ and $v = 21.2(4)$ meV for $\text{SrNi}_2\text{V}_2\text{O}_8$. Simulations based on the refined parameter values are shown as solid lines in Figs. 1–3. The fits correspond to $\chi^2 = 4.7$ for $\text{PbNi}_2\text{V}_2\text{O}_8$, and $\chi^2 = 3.8$ for $\text{SrNi}_2\text{V}_2\text{O}_8$. Given that the overall shape of the measured scans is reproduced by our model quite well, the large values of χ^2 are most likely due to the fact that experimental statistical error bars are less significant than unavoidable systematic errors, such as multiphonon scattering in the sample. While such effects can lead to an inaccurate background subtraction, they are not likely to influence the measured zone-boundary energy, as the latter is accurately pinpointed by the well-defined higher-energy cutoff in the energy scans. The relevant parameters used to fit the data, both fixed and adjustable, are summarized in Table I for both systems. The refined values for v are to be compared to previous estimates based on the measured gap energies and Eq. (5), assuming only nearest-neighbor

TABLE I. Parameters of the model Hamiltonian used to analyze the experimental data.

Parameter	PbNi ₂ V ₂ O ₈	SrNi ₂ V ₂ O ₈
Δ_{zz}	3.1 (fixed)	2.8 (fixed)
$\Delta_{xx} = \Delta_{yy}$	4.0 (fixed)	3.9 (fixed)
J_1	-0.17 (fixed)	-0.17 (fixed)
α	1.1 (fixed)	1.1 (fixed)
v	20.6(7)	21.2 (4)

interactions, $v = 22.5(1.0)$ meV and $v = 21.5(0.9)$ meV, for PbNi₂V₂O₈ and SrNi₂V₂O₈, respectively.⁴ For comparison, the dashed lines in Figs. 1 are simulations based on these latter values for PbNi₂V₂O₈.

It was important to verify that any uncertainty that may exist for the dispersion asymmetry parameter α does not have a significant impact on our determination of v . This was done by analyzing the PbNi₂V₂O₈ data using a larger value $\alpha = 0.58v$, as previously experimentally determined for NENP,¹³ rather than $\alpha = 0.44v$. Essentially the same quality of fits was obtained, and the refined spin-wave velocity $v = 19.9(8)$ meV is within the error bar of that obtained with $\alpha = 0.44v$, as described above. This demonstrates that the data analysis procedure employed is fairly insensitive to dispersion asymmetry.

We see that any deviations from the model involving only nearest-neighbor interactions are small in either material. While for SrNi₂V₂O₈, within the error bars, the discrepancy is undetectable, for PbNi₂V₂O₈ it appears to be more substantial. It is gratifying to see that for the latter system, the bandwidth measured in this work is in excellent agreement with estimates based on the high-temperature susceptibility (see above). As explained in the previous section, the reduction of zone-boundary energy is a sign of antiferromagnetic NNN in-chain interactions. Using Eq. (10) for PbNi₂V₂O₈ we obtain $J'/J \approx 0.05(2)$ and $J' \approx 0.7(3)$ meV. Detecting such small values of J' is only possible due to the large staggered susceptibility of a Haldane spin chain (the gap is relatively small compared to v) and, hence, the large prefactor in Eq. (10).

IV. DISCUSSION

To summarize, the previously proposed nearest-neighbor model for PbNi₂V₂O₈ and SrNi₂V₂O₈ should be an adequate description of these compounds in most cases, in the entire Brillouin zone. For PbNi₂V₂O₈ the data suggest, barely outside the error bars, a small antiferromagnetic NNN in-chain coupling of a few tenths of a meV. But how strong should this coupling be to have an impact on long-range ordering in a doped material? We shall now discuss the general significance of NNN interactions to spin-vacancy-induced order in weakly coupled integer-spin quantum chains and then consider the particular case of PbNi₂V₂O₈.

A. Interactions between end-chain spins

The problem of spin-vacancy-induced ordering in coupled integer-spin quantum chains with *only* nearest-neighbor in-

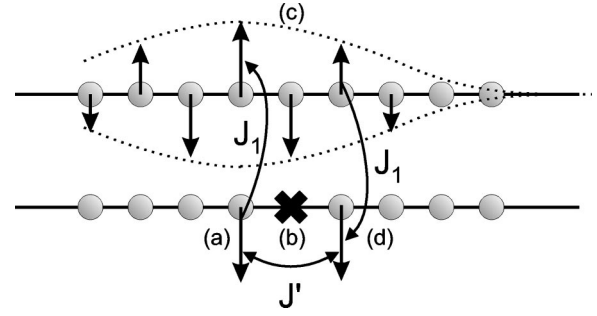


FIG. 4. A schematic representation of magnetic interactions around a nonmagnetic impurity site. End-chain $S=1/2$ degrees of freedom [(a) and (d)] appear to either side of the impurity site (b). For simplicity, the delocalized nature of these end-chain spins is not shown. The interaction J_1 of a liberated spin (a) with a neighboring chain locally polarizes the latter, inducing a “pocket” of staggered magnetization (c). The induced magnetization, in turn, couples to the other free spin (d). The resulting effective coupling competes with direct next-nearest-neighbor in-chain interactions J' .

chain interactions has been studied theoretically by Shender and Kivelson.⁹ The introduction of a nonmagnetic impurity in place of an $S=1$ ion produces two free $S=1/2$ spins located on the two ends of the severed chain.^{5–8} In each of the two fragments the end-chain spin is delocalized on a length scale defined by the intrinsic equal-time correlation length $\xi \approx 6$ of a Haldane spin chain. In principle, existing 3D interactions in the system should lead to long-range magnetic ordering of these liberated end-chain spins at a nonzero temperature.

The most interesting result of Ref. 9 is that if interchain interactions are below the threshold value at which even the undoped system orders in three dimensions, there must be a critical spin-vacancy concentration x_c below which the system remains disordered at $T=0$. The mechanism of this behavior is illustrated in Fig. 4, which show spins in the vicinity of one nonmagnetic impurity. For simplicity, the delocalized nature of end-chain spins is not shown. By virtue of interchain coupling J_1 the end-chain spin on one of the fragments of the severed chain induces a “pocket” of staggered magnetization on a neighboring chain. The size of the pocket is determined by the correlation length ξ . The induced staggered moment interacts (again via J_1) with the end-chain spin on the other fragment. This adds up to an effective second-order coupling between end-chain spins of the order of $|J'_{\text{eff}}| \approx z\chi_{\pi}J_1^2$, where z is the interchain coordination number. In Ref. 9 it is argued that this coupling is antiferromagnetic and will bind the two end-chain spins into a nonmagnetic singlet. As a result, the system will remain in a singlet ground state despite the introduction of a vacancy. Another way of looking at this phenomenon is that the effective NNN interaction J'_{eff} “patches” the broken Haldane chain at the impurity site with an antiferromagnetic bond, albeit a weak one.

We believe that this argument is, in general, incorrect. Indeed, from Fig. 4 it is clear that, no matter what the sign of J_1 is, J'_{eff} is actually *ferromagnetic* ($J'_{\text{eff}} < 0$) and, if anything, binds the two end-chain spins into a *magnetic triplet*, delo-

calized over the length scale ξ . Thus, in the absence of NNN interactions, long-range ordering should occur for arbitrary small impurity concentration x . The ordering temperature will, of course, be exponentially small with x .

This conclusion has to be modified in the presence of actual in-chain NNN AF interactions. For $J' \geq |J'_{\text{eff}}|$ the arguments of Ref. 9 can be repeated verbatim to show that the system will remain disordered at $T=0$ for sufficiently small x . On the other hand, the doped system will order at a non-zero temperature for $J' \leq |J'_{\text{eff}}|$. At any given small concentration there will be a quantum phase transition from a disordered to ordered state at a critical strength of J' given by

$$J'_c \approx z\chi_\pi J_1^2. \quad (12)$$

These estimates are semiquantitative at best, yet they provide a simple physical picture and emphasize the relevant energy scales.

B. Application to $\text{PbNi}_2\text{V}_2\text{O}_8$

In $\text{PbNi}_2\text{V}_2\text{O}_8$, which remains in a gapped state at $T \rightarrow 0$, long-range ordering can be induced by substituting some of the $S=1$ Ni^{2+} ions with nonmagnetic Mg^{2+} ions.² The transition was observed for all Mg concentrations x ranging from 0.1 down to 0.01.³ Though the Néel temperature T_N was found to decrease rapidly with decreasing x , there is, to date, no clear evidence of a critical concentration x_c below which the system remains disordered. The fact that in $\text{PbNi}_2\text{V}_2\text{O}_8$ doping-induced ordering is related to end-chain spins has been elegantly demonstrated by comparing the effects of Mg^{2+} ($S=0$) and Cu^{2+} ($S=1/2$) substitution on the Ni sites. The latter is exactly half as effective, in terms of the effect on magnetic susceptibility, since the Cu spin and the two end-chain spins become bound in a doublet state. In contrast with $S=0$ impurity substitution, the introduction of a $S=1/2$ impurity produces only one, not two, free spins in the system.²

To estimate the critical strength of NNN AF interactions that would interfere with long-range ordering in weakly doped $\text{PbNi}_2\text{V}_2\text{O}_8$, we have to estimate J'_{eff} . Using the experimental values of J and assuming $z=2$,⁴ from Eqs. (12) and (5)–(7) we obtain $J_c = |J'_{\text{eff}}| = 0.18(6)$ meV. Given the

experimental error bars and the semiquantitative nature of Eq. (12), we can only conclude that, in $\text{PbNi}_2\text{V}_2\text{O}_8$, J' [experimental value 0.4(2) meV] is of the same order of magnitude as the critical value J'_c . The question of whether there is a critical doping level below which $\text{PbNi}_2\text{V}_2\text{O}_8$ remains disordered stays open. Hopefully, extending the $T_N(x)$ measurements to lower concentrations, more accurate single-crystal neutron scattering measurements of the gap energies, and the development of a quantitative theoretical model will resolve this interesting issue in the future.

V. CONCLUSIONS

(i) This work provides a direct and accurate measurement of the zone-boundary energy in $\text{PbNi}_2\text{V}_2\text{O}_8$ and $\text{SrNi}_2\text{V}_2\text{O}_8$. The previously proposed model, based on weakly interacting $S=1$ quantum spin chains with nearest-neighbor interactions, is shown to be an adequate description of these compounds in the entire dynamic range of magnetic excitations. (ii) Unlike what was thought previously, weakly coupled Haldane spin chains should order in three dimensions at *arbitrary small* concentrations of nonmagnetic impurities. (iii) Next-nearest-neighbor AF interactions can inhibit long-range ordering at small impurity concentrations, but only if they exceed a certain critical value J'_c . (iv) In the particular case of $\text{PbNi}_2\text{V}_2\text{O}_8$, NNN interactions, if at all present, are no larger than several tenths of a meV and may be of the same order of magnitude as J'_c .

ACKNOWLEDGMENTS

We would like to thank Y. Uchiyama and I. Tsukada for the collaboration in the early stage of this study, A. Tsvetik for fruitful discussions, and B. Taylor, R. Roth, and K. Mohanty for technical support. The work at Brookhaven National Laboratory was carried out under Contract No. DE-AC02-98CH10886, Division of Material Science, U.S. Department of Energy. The work at the University of Tokyo was partially supported by a Grant-in-Aid for COE Research “SCP Project” from the Ministry of Education, Science, Sports and Culture. Oak Ridge National Laboratory is managed for the U.S. DOE by Lockheed Martin Energy Research Corporation under Contract No. DE-AC05-96OR22464.

*Present address: Oak Ridge National Laboratory, Bld. 7692, MS 6393, P.O. Box 2008, Oak Ridge, TN 37831.

¹F. D. M. Haldane, Phys. Lett. **93A**, 464 (1983); Phys. Rev. Lett. **50**, 1153 (1983).

²Y. Uchiyama, Y. Sasago, I. Tsukada, K. Uchinokura, and A. Zheludev, Phys. Rev. Lett. **83**, 632 (1999).

³K. Uchinokura, Y. Uchiyama, T. Masuda, Y. Sasago, I. Tsukada, A. Zheludev, T. Hayashi, N. Miura, and P. Boni, Physica B **284–288**, 1641 (2000).

⁴A. Zheludev, T. Masuda, I. Tsukada, Y. Uchiyama, K. Uchinokura, P. Boni, and S.-H. Lee, Phys. Rev. B **62**, 8921 (2000).

⁵I. Affleck, T. Kennedy, E. H. Lieb, and H. Tasaki, Phys. Rev. Lett. **59**, 799 (1987); Commun. Math. Phys. **115**, 477 (1998).

⁶M. Hagiwara, K. Katsumata, and I. Affleck, Phys. Rev. Lett. **65**, 3181 (1990).

⁷S. H. Glarum, S. Geschwind, K. M. Lee, M. L. Kaplan, and J. Michel, Phys. Rev. Lett. **67**, 1614 (1991).

⁸P. P. Mitra, B. I. Halperin, and I. Affleck, Phys. Rev. B **45**, 5299 (1992).

⁹E. F. Shender and S. A. Kivelson, Phys. Rev. Lett. **66**, 2384 (1991).

¹⁰Y. Uchiyama (unpublished x-ray diffraction data).

¹¹R. Wichmann and H. Müller-Buschbaum, Rev. Chim. Miner. **23**, 1 (1986).

¹²A. Zheludev, G. Shirane, Y. Sasago, N. Koide and K. Uchinokura, Phys. Rev. B **54**, 15 163 (1996).

¹³S. Ma, C. Broholm, D. H. Reich, B. J. Sternlib, and R. W. Erwin, Phys. Rev. Lett. **69**, 3571 (1992).

¹⁴I. A. Zaliznyak, S.-H. Lee, and S. V. Petrov, Phys. Rev. Lett. **87**, 017202 (2001).

- ¹⁵M. Takahashi, Phys. Rev. Lett. **62**, 2313 (1989); Phys. Rev. B **48**, 311 (1993); **50**, 3045 (1994).
- ¹⁶O. Golinelli, Th. Jolicoeur, and R. Lacaze, Phys. Rev. B **46**, 10 854 (1992); J. Phys.: Condens. Matter **5**, 1399 (1993).
- ¹⁷Stephan Haas, Jose Riera, and Elbio Dagotto, Phys. Rev. B **48**, 3281 (1993).
- ¹⁸E. S. Sørensen and I. Affleck, Phys. Rev. B **49**, 15 771 (1994).
- ¹⁹M. J. Cooper and R. Nathans, Acta Crystallogr. **23**, 357 (1967).